Prompt Tsunami Loss Estimation Using Satellite Imagery

Katsuichiro Goda
Associate Professor, Dept. of Earth Sciences, University of Western Ontario, London, Canada

ABSTRACT: This study explores the development of prompt tsunami loss estimation methods that are based on inundation hazard parameters inferred from remotely-sensed images. Using a tsunami catastrophe model for the Tohoku region of Japan, approximate tsunami loss functions are derived for coastal communities in Miyagi Prefecture. Calibration of the prompt tsunami loss estimation models is carried out by utilizing predicted tsunami losses for 4000 stochastic earthquake scenarios of moment magnitudes between M_w7.5 and M_w9.1. Using numerous earthquake sources facilitates the robust calibration of the developed tsunami loss functions. Special considerations are given to investigate the effects of coastal topography and the potential bias due to errors in estimating inundation parameters.

1. INTRODUCTION

A probabilistic tsunami catastrophe (CAT) model using stochastic earthquake sources, which was developed by Goda and De Risi (2017), is a new performance-based tsunami engineering tool for coastal communities. The approach is innovative as it accounts for stochastic processes of earthquake rupture and heterogeneous slip distribution and propagates these uncertainties through tsunami hazard simulations and tsunami damage assessments in deriving tsunami loss estimates. It promotes various applications ranging from regional tsunami loss estimation to improved risk management for disaster resilience. Considering rare occurrence of devastating tsunamis, realistic tsunami CAT models that have been calibrated against well-recorded historical events (e.g. 2011 Tohoku Japan tsunami) are a viable tool for developing prompt tsunami loss estimation tools based on regional tsunami hazard metrics which can be obtained from remote sensing techniques in post-disaster situations.

In the last two decades, remote sensing technology has played an important role for post-disaster hazard monitoring and risk management (e.g. Voigt *et al*. 2016). Key areas of its applications include real-time risk assessment, facilitating the quick coordinated responses to large-scale disasters. Among remotely sensed data, high-resolution synthetic aperture radar (SAR) images are advantageous because they cover a wide spatial area and are unaffected by weather conditions. Liu *et al.* (2013) used satellite images of inundated areas in Miyagi Prefecture due to the 2011 Tohoku tsunami to estimate flooded areas based on drastic changes of the backscattering coefficients between pre- and post-event SAR images. Recently, Moya *et al.* (2018) have proposed a hybrid tsunami damage evaluation method for buildings by integrating SAR images, numerical tsunami hazard simulation, and tsunami fragility curves through machine learning techniques. In future, remote sensing technology will become further advanced by improving timely acquisition of higher-resolution images and accurate estimation of building damage immediately after a tsunami disaster.

This study explores the development of alternative tsunami loss estimation approaches that are based on inundation depths or inundation areas inferred from satellite images. Using the probabilistic tsunami loss model for the Tohoku region of Japan (Goda and De Risi 2017), approximate tsunami loss functions are derived for buildings in Iwanuma and Onagawa. Calibration of the quick tsunami loss functions is carried out by utilizing predicted tsunami losses for 4000 stochastic earthquake rupture scenarios having M_w7.5 and M_w9.1. Using numerous

earthquake sources in calibration leads to robust quick tsunami loss estimation tools. Special considerations are given to investigate the effects of coastal topography (plain versus ria) and the potential bias due to errors in inundation parameters on the estimated tsunami loss.

2. TSUNAMI CATASTROPHE MODEL

The tsunami CAT model used consists of eight modules. Five of these components are for determining the tsunami inundation hazard across an affected region. Three remaining modules consist of an exposure model, vulnerability model, and loss calculation engine (Figure 1).

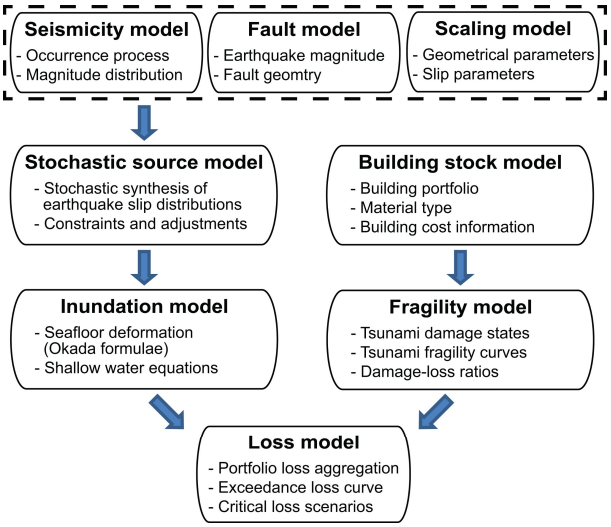

Figure 1: Tsunami loss estimation procedure.

Seismicity model The expected distribution of earthquake occurrences is characterized in accordance with the seismic hazard model for the Tohoku region proposed by the Headquarters for Earthquake Research Promotion (2013). Using earthquake catalog data in the Tohoku region, the annual occurrence rate of tsunamigenic earthquakes having M_w7.5 is estimated to be 0.08. A Gutenberg-Richter curve is fitted to obtain the recurrence values for events between M_w7.5 and M_w9.1, which are discretized with a 0.2 interval.

Fault model A regional fault source model is developed by extending the fault plane geometry for the 2011 Tohoku earthquake covering an area of 650 km long by 250 km wide. The strike angle is constant at 193º, while the dip angle is considered variable along the subducting plate interface, gradually steepening from 8º to 16º in the down-dip direction. The eastern boundary of the fault plane model approximately coincides with the Japan Trench. To characterize heterogeneous earthquake slip over the fault plane, the source zone is discretized into sub-faults of 10km by 10km in area.

Scaling model Eight source parameters are used to characterize the earthquake rupture in terms of fault geometry and slip distribution (Goda *et al*. 2016). The geometrical parameters, i.e. fault width and fault length, determine the size of the fault rupture, and the position of the synthesized fault plane is determined such that it fits within the source zone. The slip parameters, i.e. mean slip and maximum slip, specify the earthquake slip statistics over the fault plane. The Box-Cox power transformation parameter determines how the slip values are marginally distributed over the fault plane and is used to capture non-normal characteristics of earthquake slip (Goda *et al*. 2014). The spatial slip distribution parameters, i.e. correlation length along dip/strike and Hurst number, are used to characterize the heterogeneity of earthquake slip over the fault plane, represented by the von Kármán wavenumber spectrum.

Stochastic source model After sampling the spatial slip distribution parameters, a random slip field is generated using the Fourier integral method (Goda *et al*. 2014), where the amplitude spectrum is represented by the von Kármán spectrum and its phase is uniformly distributed between 0 and 2π. To achieve a slip distribution with realistic right-heavy tail features, the synthesized slip distribution is converted via Box-Cox power transformation. The transformed slip distribution is then adjusted to achieve the target mean slip and to avoid very large slip values exceeding the target maximum slip.

Inundation model To evaluate inundation depths at building locations, nonlinear shallow water equations are evaluated (Goto *et al.* 1997) by considering initial water surface elevation due to the earthquake rupture. The computational

domains are nested at four grid resolutions: 1350-m, 450-m, 150-m, and 50-m domains (note that land elevation data are represented by 50-m grids). The simulated tsunami wave heights at the grid points are used to estimate inundation depths at building locations. Inundation simulations are conducted for all stochastic sources.

Building stock model The exposure model characterizes the assets at risk within a region of interest. The building dataset used in this study is based on the post-2011-Tohoku tsunami damage data compiled by the Ministry of Land Infrastructure and Transportation (MLIT). The data contain information on building locations, damage levels based on post-tsunami surveys (minor, moderate, extensive, complete, or collapse, as defined by the MLIT), structural material (reinforced concrete, steel, wood, and others), and the number of stories. Regional statistics of unit building costs and floor areas are used to estimate the cost of the buildings, both of which are modeled as lognormal variables.

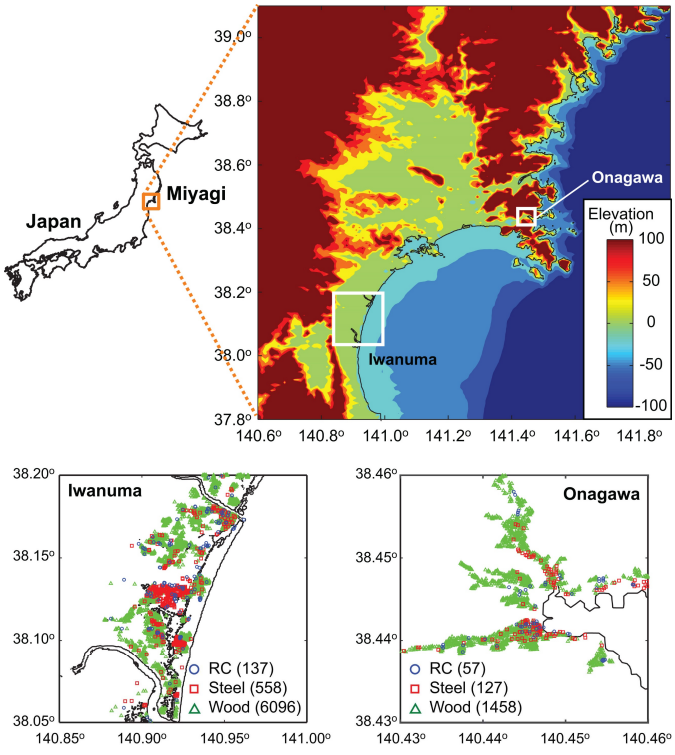

Figure 2: Building distributions in Iwanuma and Onagawa.

Fragility model Tsunami fragility functions relate tsunami hazard intensity measures (inundation depths) to probabilities of attaining different damage states. In this study, we adopt the empirical model by De Risi *et al.* (2017), which is based on the tsunami damage data gathered by the MLIT. Sampling a uniform random variable ranging between 0 and 1 and subsequently comparing this simulated value with the damage state probabilities, the corresponding tsunami damage state can be determined. According to the MLIT, damage ratios for the minor, moderate, extensive, complete, and collapse damage states are assigned as: 0.03–0.1, 0.1–0.3, 0.3–0.5, 0.5–1.0, and 1.0, respectively.

Loss model The monetary loss associated with the tsunami effect on a building is calculated by sampling the total replacement cost from the lognormal distribution and multiplying it by the damage ratio determined from the fragility analysis. The procedure is repeated for all buildings in the portfolio to obtain the total tsunami loss for each event in the stochastic sample. These loss samples can then be used to construct the conditional probability distribution functions of the total portfolio loss for a given magnitude range, and to develop the unconditional probability distribution function of tsunami loss by considering the regional seismicity.

3. PROMPT TSUNAMI LOSS ESTIMATION

To predict regional tsunami loss immediately after a major tsunamigenic event, prompt tsunami loss estimation methods take advantages of proxy tsunami hazard metrics. Availability of tsunami hazard parameters is the prerequisite for a viable rapid loss estimation method. Inundation height and inundation area over a region can be evaluated based on post-tsunami images that are obtained from remotely sensed data (e.g. Liu *et al.* 2013). Two methods that are investigated herein are based on representative inundation height and inundation area.

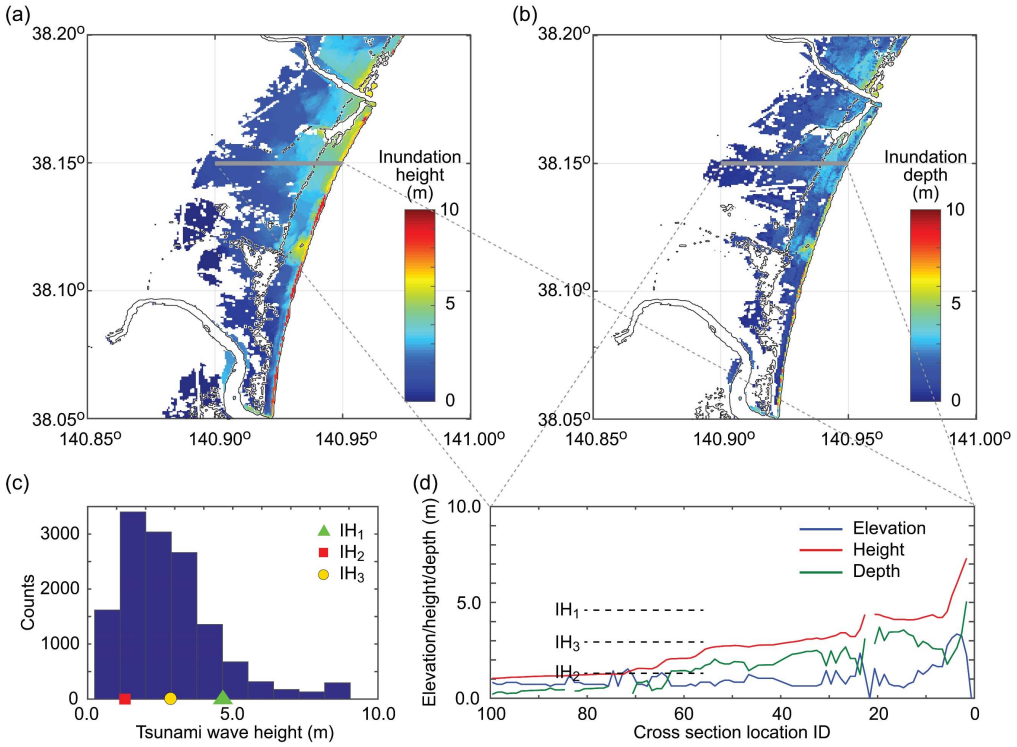

Figure 3: Tsunami inundation characteristics for Iwanuma due to a M9.0 earthquake: (a) inundation height map, (b) inundation depth map, (c) histogram of inundation height at inundated cells, and (d) cross-sectional profiles of elevation, inundation height, and inundation depth.

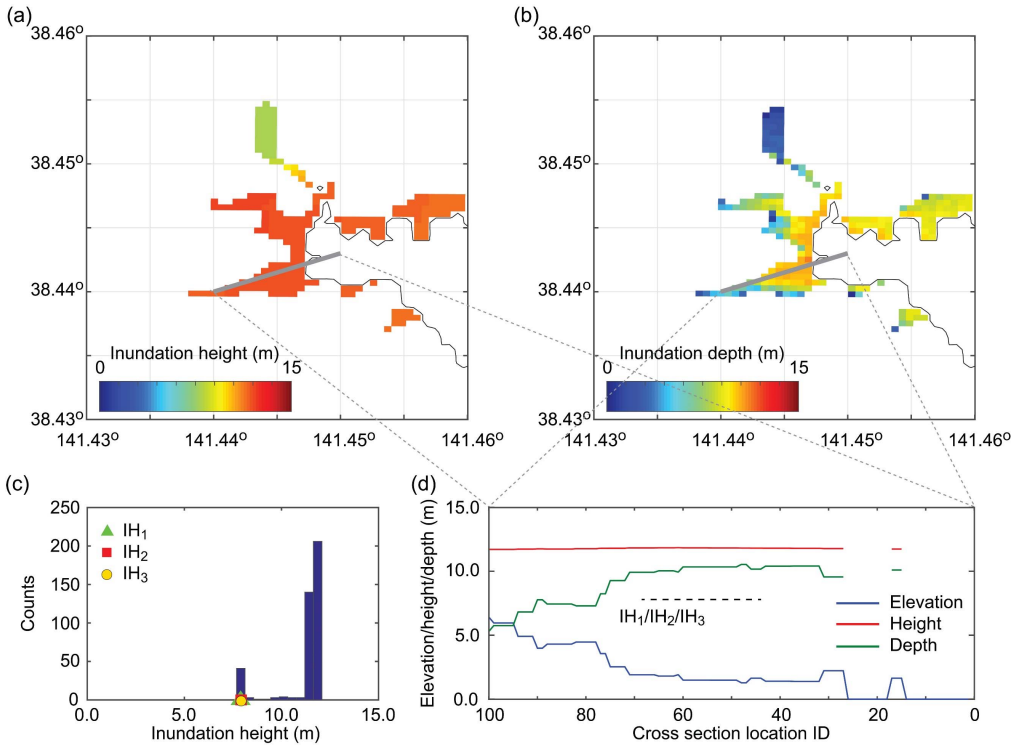

Figure 4: Tsunami inundation characteristics for Onagawa due to a M9.0 earthquake: (a) inundation height map, (b) inundation depth map, (c) histogram of inundation height at inundated cells, and (d) cross-sectional profiles of elevation, inundation height, and inundation depth.

Developing a prompt tsunami loss estimation method requires a calibration of a loss function based on surrogate tsunami hazard metrics. For such purposes, numerous pairs of tsunami hazard parameters (e.g. onshore run-up/inundation height and inundation area) and corresponding tsunami losses in a region of interest are needed. Because empirical tsunami loss data are insufficient in covering tsunami scenario characteristics in terms of rupture and magnitude comprehensively, using tsunami loss samples generated from a well-calibrated CAT model is the only viable solution. In this study, benchmark tsunami hazard estimates are set to inundation depths evaluated through tsunami wave propagation and inundation simulations by solving NSWE using 50-m grid resolutions for land areas.

With the data pairs of intensity and loss parameters, relationships between them can be developed via regression analysis. A linear regression method is deemed to be sufficient because the main purpose of this investigation is to compare the overall performances of rapid tsunami loss estimation methods based on different proxy tsunami hazard metrics. The considered functional form is:

$$log_{10}L_T = a_0 + \sum_{i=1}^{n} a_i log_{10} IM_i + \varepsilon \quad (1)$$

where L_T is the regional tsunami loss for a given building portfolio, IM_i (i = 1,…,n) are surrogate tsunami intensity parameters, a_0,…,a_n are regression coefficients, and ε is the regression error. A superior model results in smaller standard deviations of the regression error (i.e. sigma).

3.1. Loss estimation based on inundation height

A prompt tsunami loss estimation method that is investigated in this section considers single representative inundation height for a region. There are various ways to define such a representative inundation height for an area. Because inundation depths cannot be estimated directly from remote sensing images, this inundation height needs to be defined based on the elevation of inundated locations. Once the representative inundation height is determined, inundation depths at building sites can be estimated by subtracting local elevations from the (uniform) inundation height.

Three representative inundation heights are investigated by focusing on run-up front cells, which are defined as shallowly inundated locations having water depths between 0.1 m and 0.5 m. Among all run-up front cells, IH_1 is the maximum elevation, whereas IH_2 is the mean elevation. IH_3 is the average of IH_1 and IH_2. Different definitions of representative inundation height are possible by adopting different quantiles and/or by considering different subsets of inundated cells. Performances of the IH_1, IH_2, and IH_3 approximations with respect to the reference case based on NSWE (IH_{NSWE}) depend on the coastal topography and the extent of inundation. These approximate methods are intended for regional-scale assessments, rather than site-specific assessments.

To demonstrate the above-mentioned procedures of determining representative inundation heights IH_1, IH_2, and IH_3, tsunami inundation characteristics in Iwanuma and Onagawa due to a M_w9.0 scenario are focused upon, and are displayed in Figures 3 and 4. Each figure contains (a) maximum inundation height map, (b) maximum inundation depth map, (c) histogram of maximum inundation height at inundated cells (obtained from (a)), and (d) cross-sectional profiles of elevation, inundation height, and inundation depth along the line indicated in (a) and (b) (100 equally spaced points are defined along the line). The representative inundation heights IH_1, IH_2, and IH_3 are indicated in (c) and (d). The results show the effects of regional topography on tsunami inundation clearly. For Iwanuma, the topography is flat (Figure 2) and thus the maximum inundation height decays with distance from shoreline monotonically (Figure 3a,d) because of the spreading of the water over the area and the loss of run-up energy due to ground friction. As a result, a uniform representative inundation height does not capture inundation height distribution at individual sites (Figure 3d). By contrast, the maximum inundation height profile in Onagawa is nearly constant

because the entire bay area is submerged by the water (Figure 4a,d). Consequently, relative inundation depth profiles that are obtained based on IH_1, IH_2, and IH_3 resemble those based on NSWE. However, absolute values of the approximated inundation depths tend to be underestimated because IH_1, IH_2, and IH_3 are defined with respect to elevation and water depth information is missing. Although the estimates of inundation depths may be inaccurate at individual sites, the overall accuracy of the regional tsunami loss may be satisfactory. This is because prediction errors at different building sites tend to cancel one another to some extent.

To examine the tsunami loss prediction accuracy of the approximate methods based on IH_1, IH_2, and IH_3 with respect to the reference method based on IH_{NSWE}, scatter plots of tsunami loss samples based on the approximate methods and the benchmark case for all 4000 scenarios from M_w7.5 to M_w9.1 are shown in Figure 5 for Iwanuma and Onagawa. The data points along the diagonal line indicate the exact correspondence between the reference and approximate methods. Results based on IH_1 tend to overestimate the loss, whereas those based on IH_2 tend to underestimate the loss. As expected, results based on IH_3 are between these two cases and tend to be close to the diagonal line (good estimation). The results also indicate that the topographical effects of the areas are significant. For Iwanuma, differences of the approximate inundation heights can be large, whereas for Onagawa, differences are relatively small. The differences of the tsunami loss approximation performances can be explained by the topographical and run-up characteristics of the areas (Figures 3 and 4).

To quantify the prediction accuracy of the prompt tsunami loss functions based on representative inundation height IH_3, regression analyses are conducted for Iwanuma and Onagawa using Equation (1). The obtained sigma values are 0.13 and 0.06 for Iwanuma and Onagawa, respectively. The sigma values are to be compared with those based on other approximate methods.

3.2. Loss estimation based on inundation area

Alternatively, tsunami loss can be related to inundation area of a region. In this assessment, no evaluation of inundation depths is performed at individual locations. It is important to recognize some challenges in evaluating inundation areas in the post-tsunami situations. This is because when the images of the inundated areas are taken, waters have receded and not all inundated areas can be identified directly from the images. In this regard, Liu *et al*. (2013) successfully retrieved the run-up limits and inundation areas based on satellite images in a region south of Sendai (where Iwanuma is located) that were taken 2 days after the 11 March 2011 Tohoku tsunami. To account for possible variations of the estimated inundation areas, four thresholds for detecting inundated areas are considered: 0.1 m, 0.3 m, 0.5 m, and 1.0 m. For instance, for the case of 0.5 m detection threshold, it is assumed that areas that are inundated with depths greater than 0.5 m can be identified from the SAR image analysis.

Figure 6 shows scatter plots of tsunami loss samples with respect to inundation areas that are estimated based on four detection thresholds of 0.1 m, 0.3 m, 0.5 m, and 1.0 m for Iwanuma and Onagawa. The variations of the inundation areas could be regarded as possible ranges of inundation areas, and their impacts tend to be greater for coastal plain regions than for ria regions. It is important to observe that without considering the potential bias associated with the evaluation of the inundated area, the relationship between the tsunami loss and the inundation area is close to one-to-one with small variability, and such a relationship can be developed for regions with different topographies. This proves that if one can evaluate the inundation area without biases with respect to the calibrated inundation area-tsunami loss relationship, the prediction of the tsunami loss will be accurate.

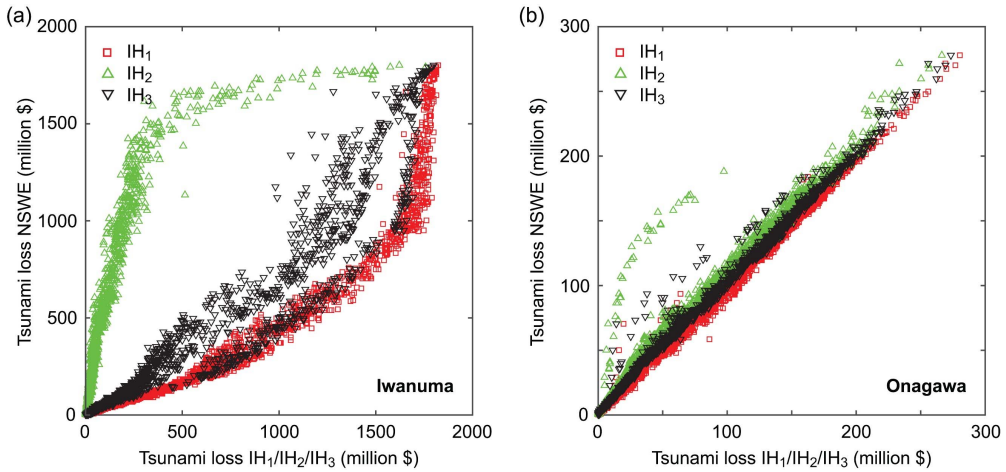

Figure 5: Comparison of tsunami-induced monetary losses based on three representative inundation heights ($IH_1/IH_2/IH_3$) and NSWE: (a) Iwanuma and (b) Onagawa.

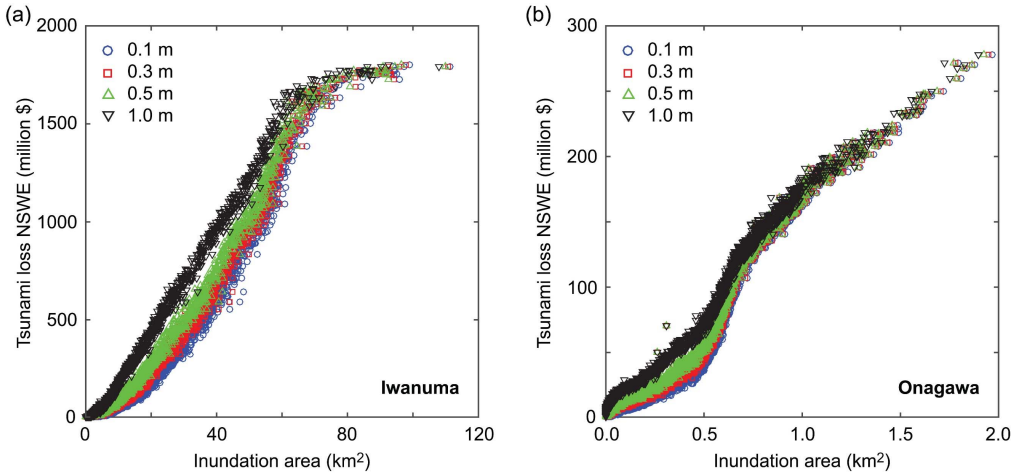

Figure 6: Comparison of tsunami-induced monetary losses based on inundation areas for different detection threshold values and NSWE: (a) Iwanuma and (b) Onagawa.

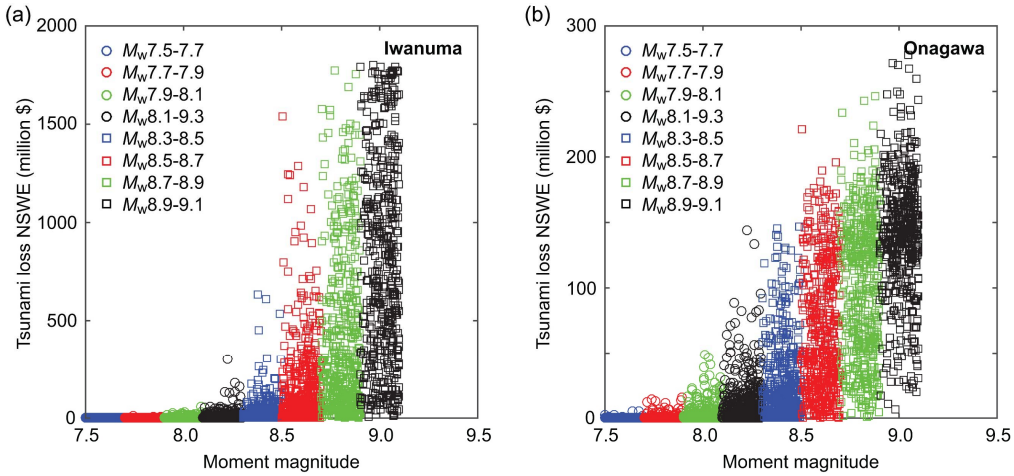

Figure 7: Comparison of tsunami-induced monetary losses based on NSWE and moment magnitude: (a) Iwanuma and (b) Onagawa.

Regression analyses of inundation areas versus regional tsunami losses are carried out to quantify the prediction accuracy by considering a case that considers single detection threshold of 0.1 m, and the other case that considers three detection threshold values (= 0.1 m, 0.3 m, and 0.5 m) as possible variation of the estimated inundation area. The former corresponds to an ideal situation where there is a high confidence in the calibrated inundation area-tsunami loss relationship, whereas the latter corresponds to a situation where uncertainty associated with the evaluation of inundation area cannot be ignored. For the single detection threshold case, sigma values are 0.11 for Iwanuma and Onagawa. When variability of the estimated inundation areas is included, sigma values increase to 0.15 and 0.18, respectively.

For comparison, additional regression analyses are performed by considering M_w as (crude) tsunami hazard measure. Because M_w is a macroscopic measure of earthquake released energy, regional tsunami loss are expected to scale with M_w broadly, which are shown in Figure 7. The sigma values calculated for the M_w-based approximate tsunami loss functions are 0.58 and 0.41 for Iwanuma and Onagawa, respectively. These sigma values are significantly greater than those calculated for the inundation-based tsunami loss functions. Indeed, the superior performances of the inundation-based methods to crude M_w-based methods can be visually inspected by comparing the results shown in Figures 5 to 7.

4. CONCLUSIONS

Prompt tsunami loss estimation methods that take advantages of proxy tsunami inundation metrics were developed. Two types of regional inundation measures, i.e. representative inundation height and inundation area, were considered, which can be evaluated based on post-tsunami images obtained from remotely sensed data. The accuracy of the approximate tsunami loss models was quantified through regression analysis. The results clearly demonstrated the potential merit of further development of the inundation-based prompt tsunami loss estimation.

5. ACKNOWLEDGEMENTS

This work is supported by the Leverhulme Trust (RPG-2017-006) and the Canada Research Chair in Multi-Hazard Risk Assessment program at Western University (950-232015).

6. REFERENCES

De Risi, R., Goda, K., Yasuda, T., and Mori, N. (2017). Is flow velocity important in tsunami empirical fragility modeling?, *Earth-Science Review*, 166, 64–82.

Goda, K., Mai, P.M., Yasuda, T., and Mori, N. (2014). Sensitivity of tsunami wave profiles and inundation simulations to earthquake slip and fault geometry for the 2011 Tohoku earthquake. *Earth, Planets and Space*, 66, 105.

Goda, K., Yasuda, T., Mori, N., and Maruyama, T. (2016). New scaling relationships of earthquake source parameters for stochastic tsunami simulation. *Coastal Engineering Journal*, 58, 1650010.

Goda, K., and De Risi, R. (2017). Probabilistic tsunami loss estimation methodology: stochastic earthquake scenario approach. *Earthquake Spectra*, 33(4), 1301–1323.

Goto, C., Ogawa, Y., Shuto, N., and Imamura, F. (1997). Numerical method of tsunami simulation with the leap-frog scheme, IOC Manual, UNESCO, No. 35, Paris, France.

Headquarters for Earthquake Research Promotion (2013). Investigations of future seismic hazard assessment, 217 p.

Liu, W., Yamazaki, F., Gokon, H., and Koshimura, S. (2013). Extraction of tsunami-flooded areas and damaged buildings in the 2011 Tohoku-Oki earthquake from TerraSAR-X intensity images. *Earthquake Spectra*, 29, S183–S200.

Moya, L., Mas, E., Adriano, B., Kshimura, S., Ymazaki, F., and Liu, W. (2018). An integrated method to extract collapsed buildings from satellite imagery, hazard distribution and fragility curves. *International Journal of Disaster Risk Reduction*, 31, 1374–1384.

Voigt, S., Giulio-Tonolo, F., Lyons, J., Kučera, J., Jones, B., Schneiderhan, T., Platzeck, G., Kaku, K., Hazarika, M. K., Czaran, L., Li, S., Pedersen, W., James, G.K., Proy, C., Muthike, D.M., Bequignon, J., and Guha-Sapir, D. (2016). Global trends in satellite-based emergency mapping. *Nature*, 353, 247–252.